SAND2021-7225C

Degradation of PERC and Al-BSF Cells with UV Cutoff and White Variations of EVA and POE Encapsulant

Alan J. Curran*, Dylan Colvin¶, Nafis Iqbal¶, Kris O. Davis¶, Thomas Moran§, Bryan D. Huey§, Brent Brownell‡, Ben Yu†, Jean-Nicolas Jaubert†, Jennifer L. Braid*‖, Laura S. Bruckman*, Roger H. French*

*SDLE Research Center, Department of Materials Science and Engineering, Case Western Reserve University, Cleveland OH, USA
†System Technology & Reliability Testing, Canadian Solar Inc. (CSI), Suzhou, Jiangsu, China
‡Cybrid Technologies Inc., Suzhou, Jiangsu, China
§Univ. of Connecticut, Storrs CT, USA
¶Univ. Central Florida, Orlando FL, USA
‖Sandia National Laboratories, Albuquerque NM, USA

***Abstract*—To assess the reliability of PERC cells compared to Al-BSF in a commercial setting minimodules with cell and encapsulant combinations are compared in accelerated exposure. In both modified damp heat and modified damp heat with full spectrum light exposures, white EVA samples showed a higher susceptibility for metallization corrosion degradation than all other encapsulants. Al-BSF cells in particular showed higher power loss than PERC cells with white EVA. It was observed that the degree of degradation had a strong significance on the manufacturer of the white EVA encapsulant. In both exposures the encapsulant was a much stronger predictor of degradation than cell type. For modules with the same encapsulant, PERC cells showed the higher performance or were comparable to Al-BSF cells for all but one case.**

***Index Terms*—I-V, accelerated exposure, degradation, PERC, data science.**

I. Introduction

Silicon solar cell technology is currently undergoing a large scale transition in industry. Traditional aluminum back-surface field cells (Al-BSF) are being replaced by a more modern cell design; the passive emitter rear contact (PERC) cell [1], [2]. As silicon makes up nearly 95% [3] of the total PV market share this represents a significant transition in the industry as a whole.

Al-BSF cells, as the name suggests, feature a continuous layer of aluminum at the back of the cell which creates a "back-surface field" that drives photon emitted charge carriers towards the surface of the cell. The back-surface field increases the performance of the cell but the aluminum silicon interface is an area of high recombination. PERC cells have a passivated rear side with a grid of aluminum contacts across the rear surface, as opposed to the continuous aluminum layer in Al-BSF. The limited aluminum-silicon contacts are still able to maintain the beneficial back-surface field while the passivatied region significantly reduces the recombination at the rear of the cell. PERC cells offer a higher conversion efficiency than Al-BSF and maintain performance with thinner wafers allowing more cells to be produced from a given amount of raw material. The similar architecture between PERC and Al-BSF allows PERC to integrate into industrial Al-BSF workflows without much disruption. PERC cells are also able to be made bifacial [4], or able to accept light from both the front and back of the cells. This has led to new types of white rear side encapsulants designed to scatter light that passes between cells into the rear of the cell, increasing the energy yield [5].

As with Al-BSF, PERC mono and bifacial cells can be made with either monocrystalline or multicrystalline silicon. Multicrystalline silicon has distinct but large grains while monocrystalline wafers are made from a single crystal [6], [7]. Mono wafers are have a higher production cost but have an improved efficiency compared to multi wafers due to fewer imperfections. Mono and multi silicon are both prevalent in the PV market, making them both relevant technologies. While many of the technologies represent a distinct trend forward in technology, i.e. Al-BSF to PERC, monofacial to bifacial, etc. mono to muticrystalline silicon is not necessarily a consistent progression. Multicrystalline silicon cells are a more modern technology but both silicon types are in use based on cost benefits [8].

From an industrial standpoint there are a large amount of new technologies being rapidly integrated into commercial panels; Al-BSF vs. PERC, monocrystalline vs. multicrystalline, monofacial vs. bifacial, as well as new white encapsu-

This material is based upon work supported by the U.S. Department of Energy's Office of Energy Efficiency and Renewable Energy (EERE) under Solar Energy Technologies Office (SETO) Agreement Number DE-EE-0008172. The views expressed herein do not necessarily represent the views of the U.S. Department of Energy or the United States Government. Sandia National Laboratories is a multimission laboratory managed and operated by National Technology & Engineering Solutions of Sandia, LLC, a wholly owned subsidiary of Honeywell International Inc., for the U.S. Department of Energy's National Nuclear Security Administration under contract DE-NA0003525.

lants paired with bifacial cells. The rapid adoption of bifacial PERC cells over Al-BSF leads to a bit of a blind spot in long term reliability studies, where there is not a backlog of historical data to rely on for estimations of long term performance for both the cells and the white encapsulants.

Additionally, prior studies of PERC cells have shown that they are more susceptible to degradation mechanisms like light induced degradation [9], [10] and light and elevated temperature induced degradation [11]–[13], and bifacial PERC cells can experience potential induced degradation from the rear side as well [14]–[16]. As such, it is important to study PERC reliability in combination with commercially relevant modern packaging materials (encapsulants or backsheets) to better understand the long term performance of these cells as they overtake Al-BSF. Studying them alongside the Al-BSF cells can help link the existing knowledge of Al-BSF degradation to estimations of the performance PERC cells into the future. Commercial relevance refers to technologies and materials (both cells and packaging polymers) that are at the forefront of industrial interest and production. In this study we investigate the degradation of commercially relevant cell and packaging combinations in accelerated exposure to compare performance of modules as a complete unit. The study is conducted using minimodules; small 4-cell modules that have the same packaging materials and cells, and are constructed the same way as full-sized commercial modules.

II. Experimental Methods

A. Sample variety

The accelerated exposures are run using minimodules as the object of study. A "minimodule" refers to a sample that is analogous to a full sized module but on a reduced scale. The smaller size allows for a greater number and diversity of cell and packaging combinations as well as easier movement and storage during exposures. The minimodules are produced with the same methods and materials as commercial full-sized modules, including production cells, inferred soldering of busbars, and lamination. All of the minimodules used in this study were produced by Canadian Solar and shipped to CWRU for exposure and measurement.

Testing samples are half-cell minimodules with the cells arranged in half-cell pairs in a two-by-two configuration, totaling eight half cells. "Half cell" refers to a solar cell that is a rectangle roughly half the size of a full cell, which are typically square. The half cells are advantageous because they operate the same as full cell but more are able to be wired in series, increasing the voltage while decreasing the current. Lower current reduces the resistive losses (proportional to I^2R) of the module under operation.

The cells are wired with each half of the module in parallel, creating two parallel sets of four half-cells in series. This configuration gives similar V_{OC} and I_{SC} magnitudes to four full cells in series when measured as a full module. Additional junction boxes were added, creating connection points between each of the four half cell pairs in the module. The extra junction boxes allow measurements to be made on the full minimodule as well as measurements of the individual cell pairs, totaling five measurement points per minimodule (full module plus four half cell pairs). As the half cell pairs are in series they have approximately double the V_{OC} and half the I_{SC} of a typical full cell measurement. This is beneficial for measurements as the higher voltage stabilizes the readings more. An image of one of the minimodules is shown in Fig. 1.

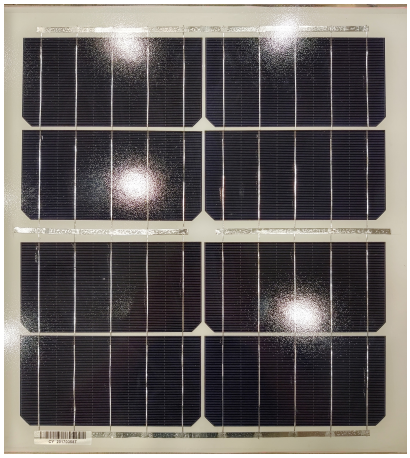

Fig. 1: Image of the front side of a half-cell minimodule. The module is divided into four pairs of cells that can be measured individually or as a whole module. Junction boxes connect to the tabs between each cell pair.

There are three types of silicon cells used in this study; multicrystalline Al-BSF, and mono and multicrystalline bifacial PERC.

The minimodules also have encapsulant varieties, along with the different cells. Ethylene vinyl-acetate (EVA) and polyolefin elastomer (POE) are the two most common commercial materials for PV encapsulation. Encapsulants are used in two layers, one in front of the cells, and another behind to surround them. The front encapsulants are UV transparent as inhibiting light transmission in front of the cell would reduce the power production of the module. The rear encapsulant, however, has UV blocking additives, making it a UV cutoff layer. This prevents UV light from reaching and degrading the backsheet of the solar panel and as the rear encapsulation is behind the cell blocking the UV transmission has no significant influence on operation. The introduction of bifacial cells has also led to white variations of these rear encapsulants to scatter light underneath said cells, increasing the power output while still protecting the backsheet from UV exposure. All minimodules have UV transparent front side encapsulants, either EVA or POE to match the rear, so any variation of encapsulant is referring to the rear side encapsulation. All four encapsulant types (white and UV cutoff EVA and POE) are represented in this sample set. For the white EVA samples there are two different suppliers, denoted as supplier 1 and supplier 2 for anonymity. All of the samples have the same KPf backsheet which has a fluoropolymer inner layer that bonds to the

encapsulant and a PVDF air facing layer bonded together with a PET core layer. A summary of all the material combinations for each of the two accelerated exposures is given in Table I.

TABLE I: Number of minimodules for each cell and encapsulant combination in the mDH and mDH+FS exposures. Individual minimodules can produce multiple results through cell level measurements.

Cell	Rear encap.	mDH count	mDH+FS count
multi Al-BSF	White EVA supp. 1	3	1
	White EVA supp. 2	0	1
	White POE	2	2
	UV cutoff EVA	0	1
	UV cutoff POE	0	1
mono PERC	White EVA supp. 1	3	1
	White EVA supp. 2	1	1
	White POE	3	2
	UV cutoff EVA	1	1
	UV cutoff POE	1	1
multi PERC	White EVA supp. 1	3	2
	White EVA supp. 2	1	1
	White POE	2	2
	UV cutoff EVA	1	1
	UV cutoff POE	1	1

Many samples have 1 minimodule with that specific combination however the junction boxes of the modules are connected in such a way that individual cell pairs can be measured. This creates a total of 5 sample measurements per minimodule, 4 half cell pairs and one full minimodule.

B. Accelerated exposures

The samples are divided between two accelerated exposures, modified damp heat (mDH) and modified damp heat with full spectrum light (mDH+FS). Distribution of the samples within each exposure is given in Table I. The exposures feature a component of mDH; a modification (hence the name) of the well known damp heat exposure in that it is run at a lower temperature of $80\ ^oC$ as opposed to the usual $85\ ^oC$. Damp heat (DH) is often criticized as being unrepresentative of real-world degradation and inducing degradation mechanisms that are not commonly observed in fielded modules. In order to better match outdoor exposure conditions we have lowered the temperature to below the glass transition temperature (T_g) of PET, a common material in backsheets. As modules typically operate around a 60-70^oC maximum, the PET in the backsheets remains well below its T_g, however a normal DH test will hold the module and consequently the PET at $85\ ^oC$ which is at the T_g. Reducing the temperature maintains a more realistic state of PET. It has been observed that DH does induces a crystallinity transition in PET that mDH exposure does not [17].

Additionally we have added a light component to one of the exposures, where the minimodules split time between the mDH and a full spectrum light chamber. Given the known susceptibility of PERC cells to LID or LeTID, light exposure is important in any comparison between PERC and Al-BSF cells. The light chamber produces a measured average irradiance of $422W/m^2$ over the surfaces of the module which totals to a dose of $1270.1MJ/m^2$ over a 168 hour step. To improve uniformity modules are rotated through positions in the light chamber at each new step.

The mDH exposure is run in seven step increments of 528 hours for a total of 3696 hours. At each point measurements are taken and the exposure is continued. The mDH+FS exposure splits time between the mDH and light chambers in a 2-1 ratio. Each step is 504 hours which equates to 336 hours of mDH and 168 hours of FS per step. In total nine steps are run, for a total of 3024 hours mDH and 1512 FS exposure.

The time spent in the environments of these accelerated exposures will be referred to as "stressors" throughout the paper. A stressor is an influence that induces change (in this case degradation) over time or cycles.

C. Stepwise measurements

At each step the minimodules are measured with both multi-sun I-V and EL/PL measurements. The I-V curves are measured using a Spire SLP4600 solar simulator at 1-sun, 0.5-suns, and 0.25 suns. Measurements are taken at both the full minimodule and cell level, totaling to five measurements per module. The electroluminescent (EL) and photoluminescent (PL) images are taken at each step as well.

After exposure the white EVA minimodules were sectioned for further analysis based on their performance. The rear side of the modules were heated and the backsheet was peeled off, then the encapsulant was cut away from the glass. This left a cutout of both the front and rear side encapsulants in the minimodule with sections taken from both the center and edges of the module for comparison. This was done for both a series of exposed modules and a control module that had not undergone any exposure.

III. Results

A. EL imaging

EL imaging shows a clear progression of corrosion in modules that experienced significant power loss. Hot humid environments like damp heat accelerated exposures are known to induce metallization corrosion in modules. Examples of imaging progression are given in Fig. 2 for different cell types in the mDH+FS exposure. Darkened regions indicate a loss of electrical connection between the metallization and the cell interface, either through an increase in series resistance or a complete dI_{SC}onnect in more serious cases. The Al-BSF cell shown in Fig. 2 in particular shows a very high degree of corrosion. EL imaging for this study is a qualitative assessment of the mechanism and progression of degradation. Performance evaluations and comparisons between samples are done via I-V measurement results.

B. Power loss modeling

There are 15 unique groups of samples when comparing the degradation performance; three cell types and five encapsulant as we treat the white EVA from different suppliers as distinct. Performance between samples is compared based on the models fitted to the trend of the power divided by

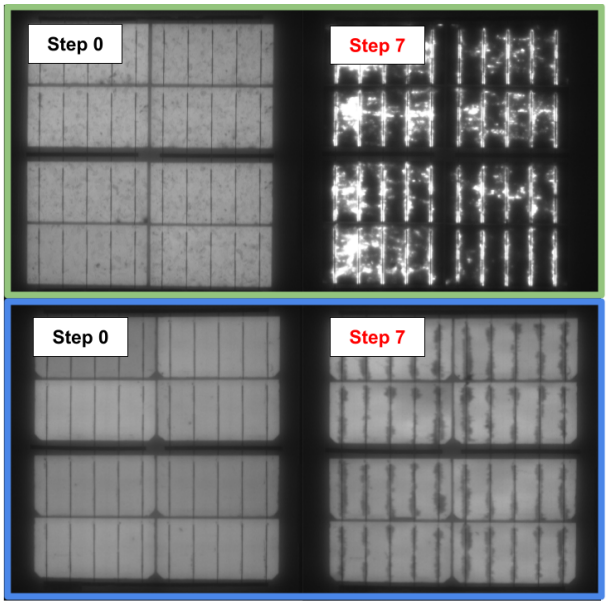

Fig. 2: Examples of EL images in samples at step 0 and step 7 of the mDH+FS exposure showing the progression of corrosion via the dark regions in the image. The top row is an Al-BSF module and the bottom row is a monocrystalline PERC module.

initial power to account for nameplate variations and cell vs. module measurements. The data and their associated models are shown in Fig. 3 for the mDH exposure and Fig. 4 for the mDH+FS exposure, with both linear and piecewise linear models fit for each cell and packaging combination. The trend in corrosion behavior is an initial stable period followed by a large drop in power and in some cases a period of low power stability afterwards. This trend is not well captured by linear models so piecewise linear models are used instead. The piecewise linear model separates a linear model into two or more linear segments which suddenly change slope at calculated changepoints, allowing it to capture non-linear trends. This model is able to capture non-linear trends while providing the high interpretability of a linear model as well a quantitative description of when a sudden change occurs within the model via the calculated changepoints.

From these piecewise linear models we can extract the predicted endpoints of all sample types and compare them quantitatively. In the specific case of the PERC-bifacial multicrystalline sample with UV POE rear encapsulant there are some significant outliers that fall below the trend of the other samples. These are caused by two of the cell pairs in the module having connection problems in their junction boxes, leading to poor I-V capture at those cell despite them operating normally. The outliers were removed when fitting the model as they are not a product of degradation and are only shown in Fig. 4.

Series resistance calculated from the DDIV R package [18] and the multi-sun I-V curves are shown in Fig. **??** for each step in the mDH+FS exposure.

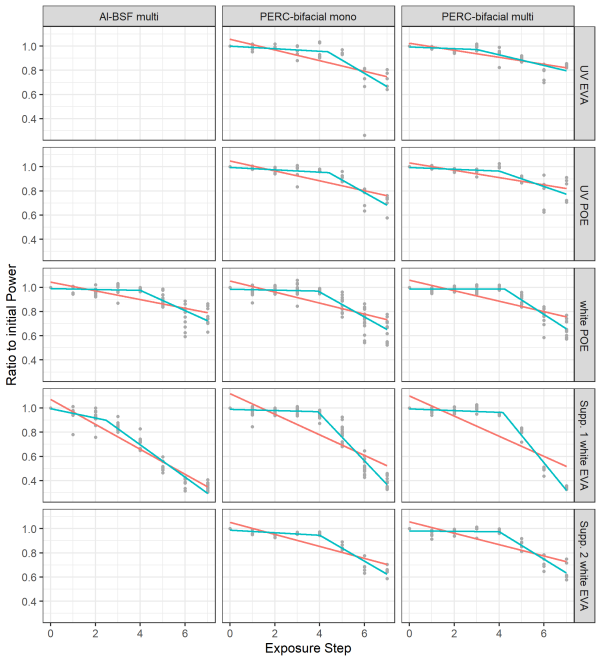

Fig. 3: Stepwise P_{mp} measurements divided by the initial power of each sample for the **mDH** exposure. Data are divided by packaging and cell combinations with linear and piecewise linear models being shown for each.

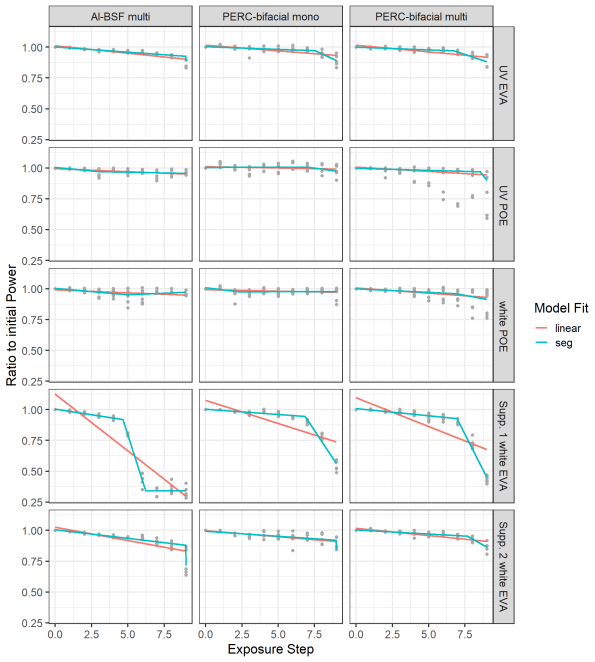

Fig. 4: Stepwise P_{mp} measurements divided by the initial power of each sample for the **mDH+FS** exposure. Data are divided by packaging and cell combinations with linear and piecewise linear models being shown for each.

C. mDH power loss results

The total fractional loss in P_{mp} based on the piecewise linear models for the mDH exposure are given in Fig. 5. The error bars shown are the 83.4% confidence intervals which indicate a $> 95\%$ confidence in mean difference between two or more distributions when the intervals do not overlap. The mDH exposure induced a significant amount of degradation in the minimodules, with the best performing sample retaining 79.6% of its initial power. The best performing samples for this exposure are the multi PERC cells with UV cutoff encapsulant variants of both EVA and POE. The other samples are lower to a statistically significant amount but they generally cluster together, indicating similar performance. All of the supplier 1 white EVA samples show considerable power loss compared to all other samples, losing more than 60% of their initial power in all cases. In particular the Al-BSF white EVA combination shows a high susceptibility to metallization corrosion. At the end of exposure all of the supplier 1 white EVA samples show a similar magnitude, however the Al-BSF samples showed a much earlier initiation of corrosion loss than the other two which saturated towards the end of the exposure while the other two caught up. The other white EVA supplier samples do not show nearly as much corrosion, being much more similar to the other encapsulants.

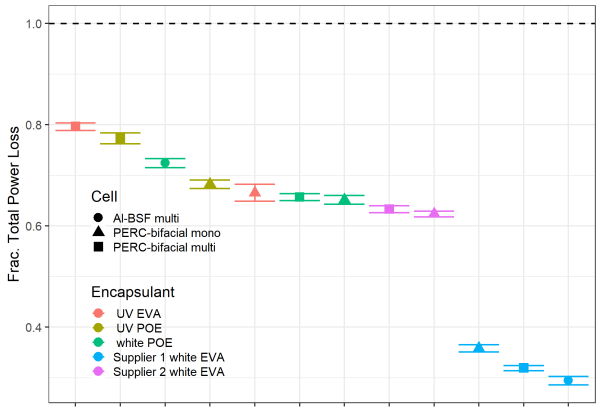

Fig. 5: Fraction of final P_{mp} compared to initial for the piecewise linear models of the mDH samples. Error bars shown are 83.4% confidence intervals.

D. mDH+FS power loss results

The power loss results for the mDH+FS Exposure are given in Fig. 6; analogous to the results discussed for mDH. Overall the mDH+FS exposure shows less power loss for most of its samples, with the best performer retaining 97.9% of its initial power. The samples cluster differently than the mDH exposure, with the best performers being both the white and UV cutoff POE samples, followed by the UV cutoff EVA, then the supplier 2 white EVA, then the supplier 1 white EVA which again shows much greater power loss than all of the other samples. The only exception to the is the UV POE/multi PERC combination which show a lower power and also a much greater variance than the other POE samples. These samples gave inconsistent measurements due to wiring problems with some of the cells, which gave lower than usual power readings. This discrepancy between cells both reduced the performance and increased the confidence intervals, but this was more due to faults within the samples not metallization corrosion. Again it is observed that the supplier 1 white EVA samples show a much greater amount of corrosion, in particular for the white EVA/Al-BSF combination. The Supplier 2 white EVA samples are more stable but the supplier 2/Al-BSF samples is beginning to show a more rapid decline compared to the other samples, but not the the extent of supplier 1.

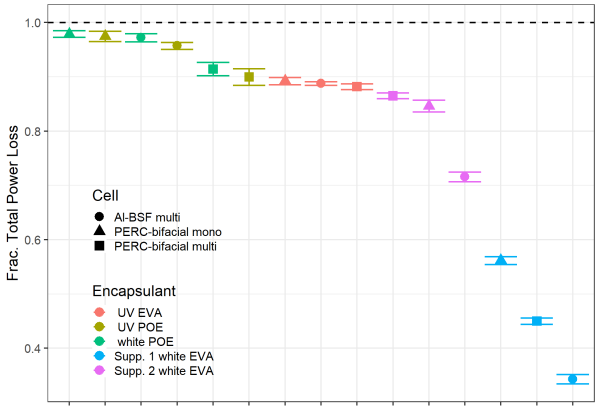

Fig. 6: Fraction of final P_{mp} compared to initial for the piecewise linear models of the mDH+FS samples. Error bars shown are 83.4% confidence intervals.

In both exposures there is a clear trend of higher risk of metallization corrosion in white EVA encapsulated samples, particularly with Al-BSF cells.

E. I-V feature degradation

The corrosive gridline degradation in the modules is expressed in other I-V features as well. Power loss is the primary indicator of degradation, but other values indicate the mechanism of power loss in the cells. A comparison between different I-V features in the white EVA modules (Fig. 7) shows the trend in the progression of degradation from other sources as well. The white EVA modules were chosen as they show the highest degree of degradation and consequently the largest signal. Other samples show similar I-V feature trends based on their degree of power loss as all samples degraded through metallization corrosion.

As expected in corrosion, the loss in power is strongly correlated with an increase in the R_S of both encapsulant suppliers. The piecewise trend in power is also observed in R_S, with a gradual increase in resistance until the changepoint where degradation rapidly accelerated and resistance increases to a greater degree. In the cases of more extreme degradation in supplier 1 there is also an associated drop in I_{SC} after a significant amount of corrosion has occurred. I_{SC} loss is not associated with small amounts of corrosion, however once

it propagates a significant amount, large areas of the cell loss their connection to the internal circuitry which leads to current loss. Initially the connections are maintained, but become more resistive through corrosive damage. In the highly degraded supplier 1 samples there is also a loss in V_{OC} which is not typically expected in damp heat tests. The relative loss is low compared to the other features (i.e. a 2% drop in V_{OC} vs a 30% drop in I_{SC} for the supplier 1 Al-BSF white EVA modules) but still suggests that recombination is increased at high levels of corrosion. The increase in recombination implies the passivation regions in the cell are beginning to degrade along with the metallization.

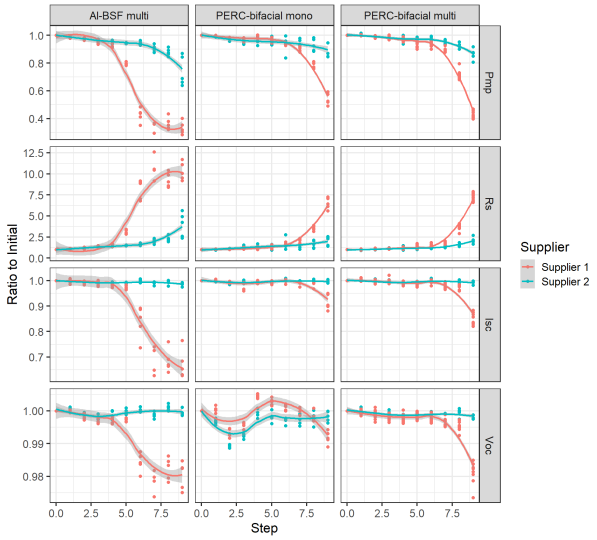

Fig. 7: I-V feature comparison for the white EVA encapsulated modules from the mDH+FS exposure. A LOESS spline is shown for each packaging combination with a 95% confidence interval. Results are normalized to the initial measurement and separated by supplier.

IV. Discussion

In both the mDH and mDH+FS exposures the mechanism inducing performance loss is metallization corrosion of the cells. In I-V features this was observed as an increase in R_s correlated with loss in P_{mp}, as well as a loss in I_{SC} at significant progression of the degradation. For the samples with the highest degradation, the R_s increase was an order of magnitude and a 30% loss in I_{SC}. This is an expected progression for metallization corrosion, which is associated with an increase in resistance as the metallization begins to degrade, with an I_{SC} loss at higher levels of corrosion when separation occurs between the metallization and the surface of the cell. There was also an observed loss in V_{OC} for the highly degraded samples, however the magnitude was much lower, at 2%. This loss in V_{OC} is most likely an increase in recombination due to passivization damage from the corrosive environment.

Quantification of degradation shows a clear ordering by module combination in both exposures. In mDH the best performers are UV cutoff encapsulants, both EVA and POE, followed by white POE, then white EVA. In mDH+FS the best performers were all the POE encapsulants, then the UV cutoff EVA, then the white EVA. Cell performance by encapsulant type was less significant than variation by encapsulants but in all cases except for one the PERC cells showed as good or better performance than Al-BSF cells with the same packaging materials. The white EVA samples were the clear outliers in terms of performance, with all white EVA modules performing worse or comparable to all other encapsulant and cell combinations. In particular the supplier 1 white EVA modules showed significantly higher degradation than the supplier 2 samples. Supplier 2 white EVA samples still had greater power loss than all other non white EVA samples but they were closer to or in some cases insignificantly different from the next best performers. The most significant observation from these exposures it the cell type is not the best indicator of degradation, with encapsulants used being a far better indicator of corrosive degradation. Additionally, the worst performer in both cases were the Al-BSF cells with supplier 1 white EVA, however the Al-BSF/white EVA combination would not be practical as Al-BSF cannot be bifacial which is the purpose of using a white encapsulant. The difference in the white EVA between suppliers 1 and 2 is currently being investigated but is unknown at this time. Overall this is promising for the transition to PERC cells as ideal selection of encapsulants gives PERC comparable to or better reliability than Al-BSF.

V. Conclusion

The rapid integration of PERC solar cells into the traditionally Al-BSF dominated marketplace has led to a reduction in the available data for PV reliability studies. As such, we have performed two accelerated exposures comparing the performance of Al-BSF and PERC cells with commercially relevant encapsulant packaging, including white and UV cutoff variants of EVA and POE. In modified damp heat (mDH) and modified damp heat with full spectrum light (mDH+FS) exposures that white EVA samples showed a much higher susceptibility to metallization corrosion for certain suppliers. Other white EVA suppliers showed much more stable performance through the exposures, indicating a manufacturing dependence on the stability of white EVA. The Al-BSF cells showed a particularly high degree of corrosion with white EVA, however this cell/packaging combination would be unrealistic for real-world systems as Al-BSF cannot be bifacial. Overall the encapsulant type of the module, not the cell type, was the best indicator of degradation in both exposures. There were inconsistencies in the best performers between the mDH and mDH+FS exposures with UV cutoff EVA performing the best in mDH while the POE samples showed the least power loss in mDH+FS. In all but one case the best or tied for best performing cells were PERC between modules with identical packaging materials; a positive result for the integration of PERC cells.

REFERENCES

[1] A. Blakers, "Development of the perc solar cell," *IEEE Journal of Photovoltaics*, vol. 9, no. 3, pp. 629–635, 2019.

[2] Jutta Trube, "International Technology Roadmap for Photovoltaic 2019," ITRPV-VDMA, Tech. Rep., Mar. 2019.

[3] Freiburg, "Photovoltaics report, updated sept. 2020," Sep. 2020.

[4] C. Deline, S. Ayala, B. Marion, B. Sekulic, M. Woodhouse, and J. Stein, "Bifacial PV System Performance: Separating Fact from Fiction," Chicago IL, 2019.

[5] M. López-Escalante, M. Fernández-Rodríguez, L. Caballero, F. Martín, M. Gabás, and J. Ramos-Barrado, "Novel encapsulant architecture on the road to photovoltaic module power output increase," *Applied Energy*, vol. 228, pp. 1901–1910, 2018.

[6] S. Glunz, R. Preu, and D. Biro, "Crystalline Silicon Solar Cells," in *Comprehensive Renewable Energy*. Elsevier, 2012, pp. 353–387.

[7] K. A. Munzer, K. T. Holdermann, R. E. Schlosser, and S. Sterk, "Thin monocrystalline silicon solar cells," *IEEE transactions on electron devices*, vol. 46, no. 10, pp. 2055–2061, 1999.

[8] C. Lan, A. Lan, C. Yang, H. Hsu, M. Yang, A. Yu, B. Hsu, W. Hsu, and A. Yang, "The emergence of high-performance multi-crystalline silicon in photovoltaics," *Journal of Crystal Growth*, vol. 468, pp. 17–23, 2017.

[9] A. Herguth, G. Schubert, M. Käs, and G. Hahn, "Investigations on the long time behavior of the metastable boron–oxygen complex in crystalline silicon," *Progress in Photovoltaics: Research and Applications*, vol. 16, no. 2, pp. 135–140, 2008.

[10] J. Lindroos and H. Savin, "Review of light-induced degradation in crystalline silicon solar cells," *Solar Energy Materials and Solar Cells*, vol. 147, pp. 115–126, 2016.

[11] K. Krauss, F. Fertig, D. Menzel, and S. Rein, "Light-induced degradation of silicon solar cells with aluminiumoxide passivated rear side," *Energy Procedia*, vol. 77, pp. 599–606, 2015.

[12] F. Kersten, P. Engelhart, H.-C. Ploigt, A. Stekolnikov, T. Lindner, F. Stenzel, M. Bartzsch, A. Szpeth, K. Petter, J. Heitmann *et al.*, "A new mc-si degradation effect called letid," in *2015 IEEE 42nd Photovoltaic Specialist Conference (PVSC)*. IEEE, 2015, pp. 1–5.

[13] E. Fokuhl, T. Naeem, A. Schmid, P. Gebhardt, T. Geipel, and D. Philipp, "Letid—a comparison of test methods on module level," in *36th European PV Solar Energy Conference and Exhibition*, vol. 36, 2019, pp. 816–821.

[14] K. Sporleder, J. Bauer, S. Großer, S. Richter, A. Hähnel, M. Turek, V. Naumann, K. K. Ilse, and C. Hagendorf, "Potential-induced degradation of bifacial perc solar cells under illumination," *IEEE Journal of Photovoltaics*, vol. 9, no. 6, pp. 1522–1525, 2019.

[15] K. Sporleder, V. Naumann, J. Bauer, S. Richter, A. Hähnel, S. Großer, M. Turek, and C. Hagendorf, "Local corrosion of silicon as root cause for potential-induced degradation at the rear side of bifacial perc solar cells," *physica status solidi (RRL)–Rapid Research Letters*, vol. 13, no. 9, p. 1900163, 2019.

[16] ——, "Root cause analysis on corrosive potential-induced degradation effects at the rear side of bifacial silicon perc solar cells," *Solar Energy Materials and Solar Cells*, vol. 201, p. 110062, 2019.

[17] M. Wang, "Degradation of photovoltaic packaging materials and power output of photovoltaic systems: Scaling up materials science with data science," Ph.D. dissertation, Case Western Reserve University, 2020.

[18] W.-H. Huang, X. Ma, and R. H. French, *ddiv: Data Driven I-v Feature Extraction*, 2018, r package version 0.1.0. [Online]. Available: https://CRAN.R-project.org/package=ddiv